PNAS Nexus, 2024, 3, 1–8
https://doi.org/10.1093/pnasnexus/pgae039
Advance access publication 30 January 2024
Research Report

The structural OFF and ON states of myosin can be decoupled from the biochemical super- and disordered-relaxed states

Vivek P. Jani[a,b,1], Taejeong Song[c,1], Chengqian Gao[d], Henry Gong[e], Sakthivel Sadayappan[c], David A. Kass[a,b], Thomas C. Irving[e,f] and Weikang Ma[e,f,*]

[a]Department of Biomedical Engineering, The Johns Hopkins School of Medicine, Baltimore, MD 21205, USA
[b]Division of Cardiology, Department of Medicine, Johns Hopkins University School of Medicine, Baltimore, MD 21205, USA
[c]Division of Cardiovascular Health and Disease, Department of Internal Medicine, University of Cincinnati, Cincinnati, OH 45229, USA
[d]College of Basic Medical Sciences, Dalian Medical University, Dalian, Liaoning 116044, China
[e]Department of Biology, Illinois Institute of Technology, Chicago, IL 60616, USA
[f]Center for Synchrotron Radiation Research and Instrumentation, Illinois Institute of Technology, Chicago, IL 60616, USA
*To whom correspondence should be addressed: Email: wma6@iit.edu
[1]V.P.J. and T.S. contributed equally to this work.
Edited By: Ivet Bahar

Abstract

There is a growing awareness that both thick-filament and classical thin-filament regulations play central roles in modulating muscle contraction. Myosin ATPase assays have demonstrated that under relaxed conditions, myosin may reside either in a high-energy-consuming disordered-relaxed (DRX) state available for binding actin to generate force or in an energy-sparing super-relaxed (SRX) state unavailable for actin binding. X-ray diffraction studies have shown that the majority of myosin heads are in a quasi-helically ordered OFF state in a resting muscle and that this helical ordering is lost when myosin heads are turned ON for contraction. It has been assumed that myosin heads in SRX and DRX states are equivalent to the OFF and ON states, respectively, and the terms have been used interchangeably. In this study, we use X-ray diffraction and ATP turnover assays to track the structural and biochemical transitions of myosin heads, respectively, induced with either omecamtiv mecarbil (OM) or piperine in relaxed porcine myocardium. We find that while OM and piperine induce dramatic shifts of myosin heads from the OFF to the ON state, there are no appreciable changes in the population of myosin heads in the SRX and DRX states in both unloaded and loaded preparations. Our results show that biochemically defined SRX and DRX can be decoupled from structurally defined OFF and ON states. In summary, while SRX/DRX and OFF/ON transitions can be correlated in some cases, these two phenomena are measured using different approaches, reflect different properties of the thick filament, and should be investigated and interpreted separately.

Significance Statement

Myosin-based thick-filament regulation is now known to be critical for muscle contraction with myosin dysregulation found in hypertrophic and dilated cardiomyopathies. While previously thought to be synonymous, this study finds that biochemical and structural thick-filament disengagements have distinct properties and should be investigated as independent phenomena. Understanding the details of thick-filament regulation will be of great relevance to defining sarcomere-level dysfunction in myopathies and understanding and better designing sarcomere therapies aimed at reversing them for treatment of cardiomyopathy.

Introduction

Regulation of vertebrate striated muscle contraction has been regarded as a calcium (Ca^{2+})-mediated thin-filament-based mechanism. Upon excitation signaling, Ca^{2+} enters the cytosol to bind to troponin-C on the thin filament, triggering a series of conformational changes to displace tropomyosin from myosin-binding sites on actin, allowing for actin-myosin cross-bridge formation and thus force generation. Initial binding of myosin to the unblocked sites results in a full cooperative activation of the thin filament to augment force (1, 2). This classical Ca^{2+}-mediated thin-filament-based regulation mechanism assumes that all myosin heads are free to bind actin once the actin-binding sites are available. However, this picture appears to be incomplete, and we now realize that muscle regulation requires both thick and thin-filament-based mechanisms to fully activate the sarcomere (3).

Thick-filament-based regulation in vertebrate muscle was first brought to our attention when Cooke and colleagues discovered

Competing Interest: W.M. and T.C.I. consult for Edgewise Therapeutics, but this activity has no relation to the current work. S.S. provides consulting and collaborative research studies to the Leducq Foundation (CURE-PLAN), Red Saree Inc., Greater Cincinnati Tamil Sangam, Affinia Therapeutics Inc., and Cosmogene Skincare Private Limited, but such work is unrelated to the content of this article.
Received: November 14, 2023. **Accepted:** January 19, 2024

that under resting conditions, myosin can exist either in a disordered-relaxed (DRX) state with a higher ATP consumption rate (~0.03 s^{-1}) or in an energy-sparing, low ATP consumption (~0.003 s^{-1}) state, known as the super-relaxed (SRX) state (4, 5). SRX and DRX are, strictly speaking, biochemically defined terms that depend on the ATP consumption rates of myosin heads. Subsequent studies suggested that myosin heads in the SRX state might be sequestered on the surface of thick filament, making them unavailable for binding to actin, whereas heads in the DRX state are free to bind to actin and generate force (6–9). The relative proportions of myosin heads in SRX and DRX states under resting conditions have been proposed to be related to the amount of force produced and to be largely responsible for the hypo- and hypercontractility observed with hereditary cardiomyopathies and more recently, end-stage heart failure (9–12). This concept motivated the development of direct myosin interventions as a therapeutic strategy to correct contractile abnormalities in myopathies culminating in the Food and Drug Administration (FDA) approval of mavacamten (Camzyos) to treat obstructive hypertrophic cardiomyopathy (13).

Another aspect of thick filament activation was brought to the forefront by Linari et al. (14), who proposed a mechanosensing-based thick filament activation model. In the resting state, the majority of the myosin heads are quasi-helically ordered on the surface of the thick filament backbone. These myosin heads, defined to be in the OFF state, produce the characteristic myosin-based layer line reflections in X-ray fiber diffraction patterns (15–17). The helical ordering is lost when myosin heads are turned ON to participate in contraction (14, 18, 19) or in response to various experimental perturbations (20–23). In the mechanosensing model, once the thin filament is turned on by influx of Ca^{2+}, a small portion of constitutively ON heads, assumed to be constantly searching for binding sites on actin, will bind to actin and generate small amounts of force that strain the thick filament. This strain then results in converting more myosin heads from the OFF state to the ON state, a behavior lost in end-stage heart failure (3, 14).

It has been generally assumed that myosin heads in the biochemically defined SRX and DRX states are equivalent to the structurally defined OFF and ON states, respectively (3, 6, 24), so that the terms SRX state and OFF state are often used interchangeably. In this study, we used X-ray diffraction and ATP turnover assays to track the structural and biochemical transitions induced by either omecamtiv mecarbil (OM) or piperine, respectively, under resting conditions. OM and piperine were chosen in this study for the following reasons: OM was the first myosin activator to undergo, ultimately unsuccessful, clinical trials as a myosin activator (25), but it was also shown to have inhibitory effects on myosin ATPase in the absence of actin (26). OM has been shown to stabilize the ON state of the thick filament (27) and activate muscle mainly by increasing the fraction of myosin heads strongly binding to the actin filaments (28, 29) at any moment (i.e. duty ratio), but no information concerning the role of OM in modulating the population of myosins in SRX/DRX state has been reported (10). Piperine, a phenol derivative of black pepper, has been shown to change the portion of myosin heads in the SRX state in fast skeletal muscle but not in slow skeletal muscle and cardiac muscle (30, 31); hence, piperine was chosen due to its ability to selectively modulate the populations of myosin in the SRX/DRX state among different muscle types. We show that while OM and piperine induce dramatic shifts of myosin heads from the OFF to the ON states in skinned porcine cardiac muscle, there are no appreciable changes in the populations of myosin heads in the SRX and DRX states. These results reveal that the biochemically defined SRX and DRX states can be decoupled from the structurally defined OFF and ON states, indicating that these behaviors do not necessarily reflect the same underlying phenomena. This new understanding is of critical clinical significance, since the presumed coupling between OFF/ON and SRX/DRX as an underlying assumption has the potential to be seriously misleading in the design of therapeutic approaches for cardiomyopathies.

Results

Structural changes of permeabilized porcine myocardium with OM and piperine

We studied X-ray diffraction patterns obtained from relaxed permeabilized porcine myocardium at different concentrations of OM and piperine under resting conditions (pCa8). Qualitatively, permeabilized porcine myocardium showed characteristic relaxed myosin-based layer lines (MLL1 and MLL2) in the absence of myosin activators, which diminished in intensity with increasing activator concentration, until they were no longer visible in the presence of the highest concentrations of OM (~10 μM) and piperine (~50 μM) used in this study (Fig. 1A and B, respectively). The equatorial intensity ratio ($I_{1,1}/I_{1,0}$), an indicator of the proximity of myosin heads to actin in relaxed muscle (15), increased monotonically as a function of either OM (Fig. 1C, Table 1) or piperine (Fig. 1D, Table 2) concentrations, indicating a shift of myosin heads away from the thick-filament backbone toward the thin filament at increased concentrations of each activator.

Both I_{MLL1} and I_{M3} decreased slightly with 0.1 μM OM treatment and further decreased monotonically (up to 70% at 10 μM OM) at higher concentrations (Fig. 2A and C, Table 1). Similarly, both I_{MLL1} and I_{M3} decreased slightly at 2 μM piperine and further decreased monotonically at higher concentrations (Fig. 2B and D, Table 1). The intensity of the sixth-order myosin-based meridional reflection (M6) arises primarily from the thick filament backbone. The spacing of M6 reflection (S_{M6}), reflecting the thick filament backbone periodicity (15), increases as the concentration of either OM or piperine increases (Fig. 2E and F, Table 1). Both an increase in the thick filament backbone periodicity, indicated by increased S_{M6}, and a reduction in the degree of the helical ordering of the myosin heads, indicated by reduced I_{MLL1} and I_{M3}, are characteristic signatures of the structurally defined OFF to ON transition of myosin (3, 15, 32). Taken together, these findings show both OM and piperine cause a substantial disruption of the helical ordering of myosin heads on the surface of the thick filament backbone, resulting in the release of myosin heads to move closer to actin; i.e. an OFF to ON transition.

Changes in the ATP turnover rate in permeabilized porcine myocardium with OM and piperine

To test the hypothesis that structurally defined OFF/ON state myosin heads are strongly correlated to biochemically defined SRX/DRX state, we next examined the proportion of myosin heads in SRX and DRX states with and without both activators. OM (5 μM) or piperine (50 μM) was applied to permeabilized myocardial strips under unloaded conditions, and the decay rate of fluorescent mant-ATP provided a measure of the ATP turnover rate. The relative proportions of the myosin heads in the DRX and SRX states and the time constant of the fast phase (T_1) and the slow phase (T_2) were calculated by fitting the fluorescence decay profile with a two-phase exponential decay function (c.f. Materials and methods). We observed overlapping fluorescence decay signals in

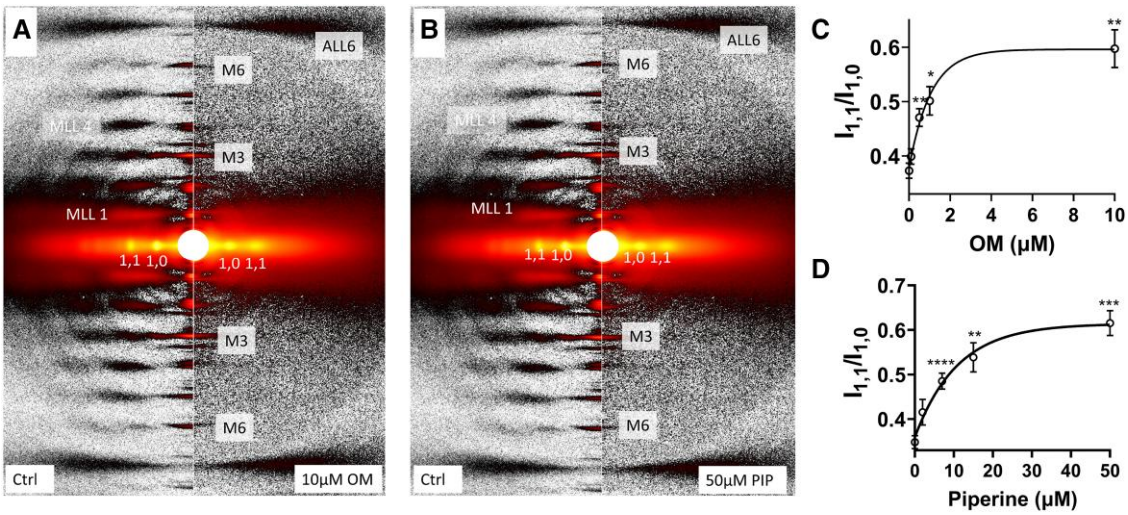

Fig. 1. X-ray diffraction patterns from permeabilized porcine myocardium in relaxing solution in the absence and presence of myosin activators. A) X-ray diffraction patterns from relaxed muscle in the absence (left panel) and presence (right panel) of 10 μM OM. B) X-ray diffraction patterns from relaxed muscle in the absence (left panel) and presence (right panel) of 50 μM piperine (PIP). Equatorial intensity ratio ($I_{1,1}/I_{1,0}$) at different concentrations of OM C) and piperine D). Myosin heads move radially closer to actin as OM and piperine concentration increases. The results are given as mean ± SEM with *P*-values were calculated from one-way repeated measures ANOVA with Dunnett's multiple comparisons test compared with control (0 μM activator). $^{*}P < 0.05$, $^{**}P < 0.01$, $^{***}P < 0.001$, $^{****}P < 0.0001$.

control (untreated) and OM/piperine-treated tissues. Neither the fraction of the myosin heads in the SRX state nor the T_1 and T_2 values change significantly in the presence of either OM or piperine (Fig. 3, Table 2).

While unloaded assays are commonly used to assess SRX/DRX transitions, it has now been shown that the population of myosin heads in SRX vs. DRX is sensitive to the sarcomere length in both porcine (28) and human myocardium (32). Sarcomere length is not controlled in unloaded assays, contributing to increased variance in the measurements. Furthermore, the diffusion of free nucleotides out of relatively large multicellular muscle bundles takes 10–15 s, overlapping with the fast-phase time constant (T_1) in the ATP turnover assay, complicating data interpretation (7). To mitigate these potential limitations, we also used a recently developed loaded ATP turnover procedure (32) in permeabilized single cardiomyocytes (CMs) and measured the proportions of myosin heads in the SRX/DRX state in paired preincubation and postincubation with both compounds of interest. Similar to the results obtained from unloaded fiber bundles, we find no significant changes in the proportion of myosin heads in the SRX state (OM $P = 0.28$; piperine $P = 0.43$) before and after OM or piperine treatment (Fig. 4, Table 2). However, we observed a significant 35% reduction (Table 2) in T_1 with 1 μM OM (Fig. 4E), suggesting that OM increases the ATPase activity of DRX myosin heads. In summary, in all cases, there were no significant changes in the fraction of the myosin heads in the SRX state despite the increase in the equatorial intensity ratio previously observed.

Discussion

It has been often observed that the structurally defined OFF and ON states of myosin are correlated with the biochemically defined SRX and DRX states (3, 6, 10, 33) and, consequently, are widely assumed to reflect the same underlying phenomena. Mavacamten, a small-molecule myosin-inhibitor-treated myocardium is one case where transitions of myosin heads from the DRX to the SRX are well correlated to ON to OFF transitions (7, 34). Additionally, it has been shown that, at least in one cohort of right ventricle heart failure patients, increases in the population of myosin heads in the biochemical SRX state and structural OFF state might be the underlying cause of depressed contractile force associated with right ventricular failure (35). Myosin activators that were able to recruit myosin from the OFF and the SRX states were, therefore, proposed to be one possible therapy for these patients. So far, only deoxy-ATP (36, 37) and EMD-57033 (32) have been shown, when used as tool compounds, to be able to recruit myosin from the OFF and the SRX states to ON and DRX states, respectively.

The structural basis for the SRX has been proposed to be the interacting head motif (IHM), in which a pair of the myosin heads interact with each other and the S2 segment causes them to be held close to the thick filament backbone (6, 38, 39). While our definition of the helically ordered OFF state does not address the precise configuration, and possible heterogeneity, of the OFF-state myosin heads, a recent cryo-EM study on isolated human cardiac thick filaments showed that there are three distinct IHM configurations that are quasi-helically ordered on the surface of the thick filament in the presence of mavacamten (40). This suggests that a substantial fraction of the myosin heads in the structurally defined OFF state in resting muscle are likely to be in one of these IHM states. Here, our X-ray diffraction data showed that an increased concentration of OM and piperine induces a dramatic reduction in the helical ordering of the myosin heads (Fig. 2), accompanied by a radial movement of the myosin heads toward actin (Fig. 1) at pCa8. These data strongly indicate an OFF to ON transition of myosin heads induced by OM and piperine. ATP turnover assays using both unloaded porcine fiber bundles and loaded cardiomyocytes, however, showed that OM and piperine did not significantly alter the relative portion of the myosin heads in the SRX and DRX states. These findings refute the notion that the biochemically defined SRX and DRX states are necessarily manifestations of the structurally defined OFF and ON states, but rather that these behaviors are distinct. We conclude that a biochemical SRX to DRX transition of myosin does not necessarily imply a structural OFF to ON transition and that a structural OFF to ON transition does not necessarily imply a biochemical SRX to DRX transition.

Table 1. X-ray diffraction pattern changes in the presence of increasing concentration of OM and piperine (PIP).

	Interpretation	0 μM OM	0.1 μM OM	0.5 μM OM	1 μM OM	10 μM OM	h-v (95% CI) μM
$I_{1,1}/I_{1,0}$	Proximity of myosin heads to actin	0.37 ± 0.014	0.40 ± 0.014	0.47 ± 0.016[a]	0.50 ± 0.026[b]	0.60 ± 0.035[a]	0.74 (0.38–1.50)
I_{MLL1} (a.u.)	Helical ordering of the myosin heads	10.76 ± 0.71	8.36 ± 0.84	6.88 ± 0.60[a]	6.16 ± 0.65[b]	3.72 ± 0.26[c]	0.56 (0.21–1.16)
I_{M3} (a.u.)	Axial ordering of the myosin heads	6.67 ± 0.50	5.52 ± 0.44	4.68 ± 0.35[a]	3.87 ± 0.19[d]	3.30 ± 0.16[d]	0.41 (0.11–0.92)
S_{M6} (nm)	Thick filament backbone periodicity	7.186 ± 0.002	7.192 ± 0.002	7.199 ± 0.002[c]	7.201 ± 0.002[a]	7.207 ± 0.002[d]	0.38 (0.13–0.78)
		0 μM PIP	**2 μM PIP**	**7 μM PIP**	**15 μM PIP**	**50 μM PIP**	**h-v (95% CI) μM**
$I_{1,1}/I_{1,0}$	Proximity of myosin heads to actin	0.35 ± 0.015	0.42 ± 0.029	0.49 ± 0.018[d]	0.54 ± 0.033[a]	0.62 ± 0.028[a]	7.55 (3.63–16.7)
I_{MLL1} (a.u.)	Helical ordering of the myosin heads	14.09 ± 1.36	9.55 ± 1.02	7.21 ± 0.88[c]	5.34 ± 0.60[a]	3.90 ± 0.54[c]	3.36 (1.34–7.56)
I_{M3} (a.u.)	Axial ordering of the myosin heads	10.12 ± 1.19	7.19 ± 1.02	5.24 ± 0.41[a]	4.25 ± 0.51[a]	3.13 ± 0.35[a]	3.29 (1.18–8.61)
S_{M6} (nm)	Thick filament backbone periodicity	7.178 ± 0.004	7.185 ± 0.003	7.191 ± 0.003[a]	7.197 ± 0.002[a]	7.200 ± 0.002[a]	5.01 (1.67–13.4)

Values are given as mean ± SEM. The *P*-values were calculated from one-way repeated measures ANOVA with Dunnett's multiple comparisons test compared with control (0 μM OM or piperine). The half value (h-v) and 95% CI were calculated by fitting the values of each reflection in a function of activator concentration to an exponential function. $n = 8$. [a]$P < 0.01$. [b]$P < 0.05$. [c]$P < 0.001$. [d]$P < 0.0001$.

Table 2. ATP turnover assay before and after either OM or piperine (PIP) treatment.

	Unloaded myocardium bundles				Loaded cardiomyocytes					
	Ctrl ($n = 15$)	**OM ($n = 11$)**	**PIP ($n = 9$)**	***P*-values**	**Ctrl ($n = 10$)**	**OM ($n = 10$)**	***P*-values**	**Ctrl ($n = 10$)**	**PIP ($n = 10$)**	***P*-values**
%SRX	49.1 ± 6.9	58.5 ± 7.1	42.32 ± 9.1	ns	47.71 ± 2.15	43.62 ± 2.75	ns	42.99 ± 4.32	38.57 ± 3.20	ns
T_1 (s)	24.20 ± 1.67	25.52 ± 1.99	27.65 ± 2.67	ns	8.74 ± 0.82	5.9 ± 0.78	<0.01	9.20 ± 1.68	7.24 ± 0.60	ns
T_2 (s)	129.6 ± 13.0	114.5 ± 14.1	145.9 ± 20.3	ns	271.5 ± 27.9	213.4 ± 41.6	ns	321.2 ± 61.3	270.9 ± 30.82	ns

The results are given as mean ± SEM, with *P*-values are calculated from unpaired Brown–Forsythe and Welch ANOVA test for unloaded myocardium bundles experiments and *P*-values calculated from Wilcoxon matched-pairs signed-rank t tests for loaded CM experiments. ns, not significant.

It is worth noting that the biochemical SRX/DRX state of myosin, by definition, reflects the myosin ATP turnover rates measured under relaxing conditions. Thus, it cannot be assessed at high Ca^{2+} concentrations, unless one can eliminate Ca^{2+}-dependent acto-myosin interaction (41), or try to disentangle the ATP consumption of force producing cross-bridges from that of the other myosin populations (5), which may not be possible in many circumstances. Here, we limited our investigations of the SRX/DRX and OFF/ON states of myosin under relaxing conditions. The possibility of a disconnect between the biochemical and the structural states of myosin has previously been reported in the literature. In relaxed porcine myocardium, while structural OFF to ON and biochemical SRX to DRX transitions both increased in response to increasing dATP concentration (36), DRX myosin heads increased linearly with increasing dATP concentration, whereas the structural OFF to ON response was nonlinear. Furthermore, Chu et al. (38) showed that mavacamten, a small-molecule myosin inhibitor, has a greater effect on the increase in the population of myosin in the SRX state than the increase in number of myosin heads in the IHM state. A recent study by Mohran et al. (42) showed that in the case of heavy meromyosin (HMM) in solution, the mant-ATP fluorescent decay curves can be fit to a single exponential, challenging the validity of using mant-ATP pulse-chase experiments to assess SRX/DRX populations in isolated proteins in solution. As stated by the authors, the results on HMM studies may not be applicable to systems with intact sarcomeres where interactions involving myosin heads, myosin tails, titin, myosin-binding protein C, and other accessory proteins, as demonstrated by recent cryo-EM studies (43, 44), will alter the stabilities of myosin states and the relative populations of SRX and DRX heads. Attempts to resolve these controversies are beyond the scope of the current study and will be addressed elsewhere.

It is clear that the biochemically defined SRX and DRX states can respond differently to physiological perturbations and experimental interventions from the structurally defined OFF and ON states and that they should not necessarily be considered to represent the same underlying phenomena. These findings have direct translational significance. First, it is clear that for any compound that might target the SRX/DRX or the OFF/ON equilibrium as a therapeutic route for both heart and skeletal muscle diseases, one cannot assume they are necessarily coupled. Second, ongoing studies in our laboratories indicate that decoupling of biochemical SRX/DRX and structural OFF/ON transitions probably occurs more widely than presented here, and rather than a peculiarity of the specific compounds studied here, the demonstration that the two phenomena do not act in lock-step is of broad physiological and pathological significance for health and disease. We suggest, therefore, that both SRX/DRX and structural OFF/ON state transition measurements should be done as part of a comprehensive study of either the mode of action of candidate therapeutic compounds or underlying disease mechanisms, to better inform further decision-making in therapeutic strategies.

Materials and methods

Muscle preparation for X-ray diffraction

Porcine left ventricle was prepared as described previously (45, 46). Briefly, frozen porcine left ventricle wall was thawed in skinning solution (pCa8 solution: 91 mM K^+-propionate, 3.5 mM MgCl, 0.16 mM $CaCl_2$, 7 mM ethylene glycol-bis(β-aminoethyl ether)-N, N,N′,N′-tetraacetic acid (EGTA), 2.5 mM Na_2ATP, 15 mM creatine phosphate, 20 mM imidazole) plus 30 mM 2,3-Butanedione monoxime (BDM), 1% Triton-X100 at room temperature for 1 h before dissection into smaller strips. Myocardium strips were skinned at room temperature for 2 h. The fiber bundles were further dissected into preparations with a length of 5 mm with a diameter of 200 μm prior to the attachment of aluminum T-clips to both ends in pCa8 solution with 3% dextran on ice for the day of the experiment. X-ray diffraction experiments were performed at the BioCAT beamline 18ID at the Advanced Photon Source, Argonne

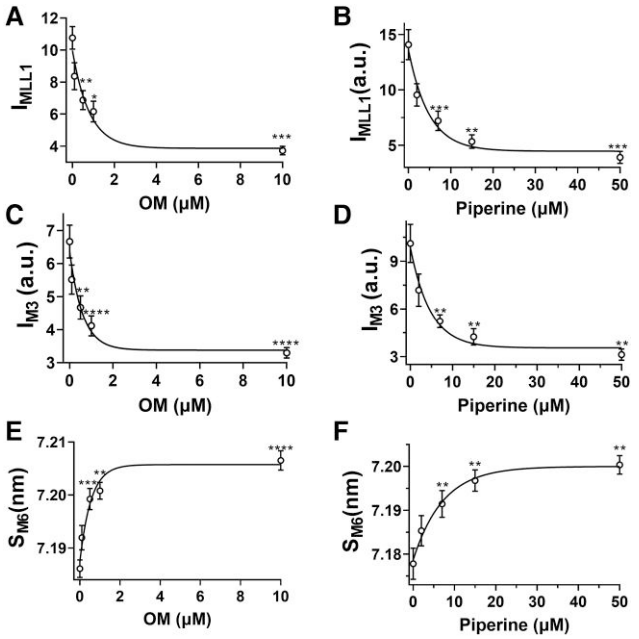

Fig. 2. Thick filament structural changes in the presence of myosin activators. The intensity of the first-order myosin-based layer line (I_{MLL1}) in different concentrations of OM A) and piperine B). The third-order myosin-based meridional reflection (I_{M3}) in different concentrations of OM C) and piperine D). The spacing of the sixth-order myosin-based meridional reflection (S_{M6}) in different concentrations of OM E) and piperine F). Myosin heads move from the helically ordered OFF states to disordered ON states as activator concentration increases. The results are given as mean ± SEM with *P*-values were calculated from one-way repeated measures ANOVA with Dunnett's multiple comparison test compared with control. $^{*}P < 0.05$, $^{**}P < 0.01$, $^{***}P < 0.001$, $^{****}P < 0.0001$.

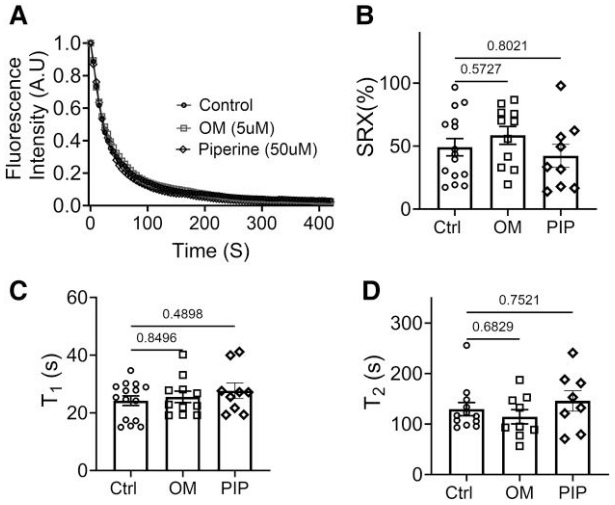

Fig. 3. ATP turnover assays of unloaded permeabilized porcine myocardium bundles treated with OM and piperine (PIP). A) Mant-ATP dissociation over time curves in control (circle symbols), 5 μM OM (square symbols), and 50 μM piperine (diamond symbols). B) The percentage of myosin heads in the SRX state (% SRX) with and without OM and piperine. C) The time constant of the fast phase (T_1) with and without OM and piperine treatment. D) The time constant of the slow phase (T_2) with and without the OM and piperine treatment. The results are given as mean ± SEM, with *P*-values as shown in the figure calculated from unpaired Brown–Forsythe and Welch ANOVA tests.

National Laboratory (47). The X-ray beam energy was set to 12 keV (0.1033 nm wavelength) and the incident flux was set to ~5×10^{12} photons/s. The specimen-to-detector distance was about 3 m. The muscle was incubated in a customized chamber with one end attached to a force transducer (Model 402B Aurora Scientific Inc., Aurora, ON, Canada) and Kapton windows in the X-ray path in pCa8 solution. The experiment was performed between 28 and 30 °C at a sarcomere length of 2.3 μm as adjusted by laser diffraction. X-ray diffraction patterns were collected on a MarCCD 165 detector (Rayonix Inc., Evanston, IL, USA) with a 1-s exposure time as a function of five increasing OM (0, 0.1, 0.5, 1, and 10 μM) and piperine (0, 2, 7, 15, and 50 μM) concentrations. OM was purchased from AdooQ Biosciences (Irvine, CA, USA), and piperine from Millipore Sigma (St Louis, MO, USA). To minimize radiation damage, the muscle was oscillated along its horizontal axes at a velocity of 1 mm/s and moved vertically after each exposure to avoid overlapping X-ray exposures. Two to three patterns were collected under each condition, and the spacings and intensities of selected X-ray reflections extracted from these patterns were averaged.

X-ray data analysis

The data were analyzed using the MuscleX software package developed at BioCAT (48). Briefly, the equatorial reflections were measured by the "Equator" routine in MuscleX, as described previously (49). The intensities and spacings of meridional and layer line reflections were measured by the "Projection Traces" routine in MuscleX, as described previously (34, 50). To compare reflection intensities under different conditions, the measured intensities of X-ray reflections were normalized to the intensities of the sixth-order actin-based layer line (36). The results are given as mean ± SEM with *P*-values were calculated from one-way repeated measures ANOVA with Dunnett's multiple comparisons test compared with control (0 μM activator). The values of each reflection as a function of activator concentration were fitted to a one-phase association function ($Y = Y0 + [\text{Plateau} - Y0] \times [1 - \exp\{-K \times x\}]$) or a one-phase decay function ($Y = [Y0 - \text{Plateau}] \times \exp[-K \times X] + \text{Plateau}$) to calculate half values and 95% CIs. Extra sum-of-square *F* tests indicate that one-phase functions are preferred to hyperbolic functions ($P < 0.0001$).

Unloaded ATP turnover assays in permeabilized porcine myocardium bundles

Permeabilized porcine cardiac tissue was prepared, as described previously (51, 52). Briefly, previously frozen porcine cardiac tissue was cut into small pieces and skinned for 6 h on ice in a skinning buffer (100 mM NaCl, 8 mM $MgCl_2$, 5 mM EGTA, 5 mM K_2HPO_4, 5 mM KH_2PO_4, 3 mM NaN_3, 5 mM ATP, 1 mM Dithiothreitol (DTT), 20 mM BDM, and 0.1% (v/v) Triton X-100 at pH 7.0). The skinning buffer was changed every 2 h. After skinning, the permeabilized fibers were placed in a glycerinating buffer overnight at 4 °C. Then, samples were stored in fresh glycerinating solution (120 mM K acetate, 5 mM Mg acetate, 5 mM EGTA, 2.5 mM K_2HPO_4, 2.5 mM KH_2PO_4, 50 mM 3-morpholinopropane-1-sulfonic acid (MOPS), 5 mM ATP, 20 mM BDM, 2 mM DTT, and 50% (v/v) glycerol at pH 6.8) at −20 °C until use. To measure the SRX/DRX state of myosin, skinned cardiac tissue was further cut into a small bundle of fibers in cold glycerol buffer. Both sides of the fiber were secured with double-sided tape in a flow chamber (thickness ~270 μm), as described previously (52). Samples were washed five times with rigor buffer (120 mM K acetate, 5 mM Mg acetate, 5 mM EGTA, 2.5 mM K_2HPO_4, 2.5 mM KH_2PO_4, 50 mM MOPS, and 2 mM fresh DTT at pH 6.8) to remove residual glycerol, ATP, and BDM in the fiber. Next, the fibers were incubated in rigor buffer containing 250 μM mant-ATP for

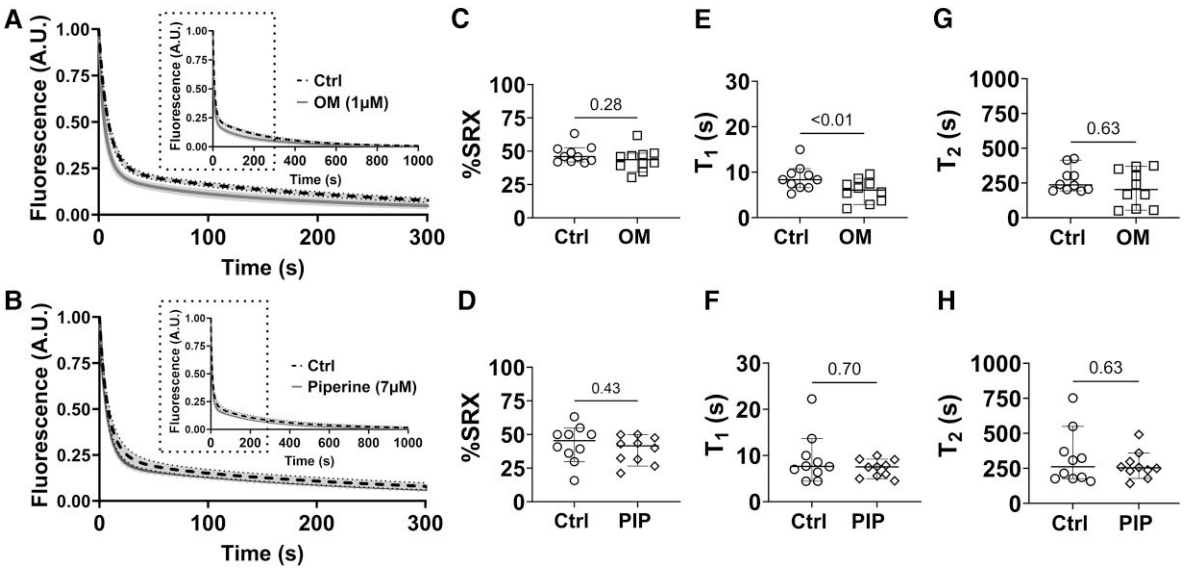

Fig. 4. ATP turnover assays of loaded permeabilized porcine CMs before and after OM and piperine (PIP) treatment. A) Mant-ATP dissociation over time curves in control (dashed line) and 1 μM OM (solid line). B) Mant-ATP dissociation over time curves in control (dashed line) and 7 μM piperine (solid line). The percentage of myosin heads in the SRX state (% SRX) before (circle symbols) and after OM (square symbols) C) and piperine (diamond symbols) D) treatment. The time constant of the fast phase (T_1) before (circle symbols) and after the OM (square symbols) E) and piperine (diamond symbols) F) treatment. The time constant of the slow phase (T_2) before (circle symbols) and after the OM (square symbols) G) and piperine (diamond symbols) H) treatment. The results are given as mean ± SEM with *P*-values as shown in the figure calculated from Wilcoxon matched-pairs signed-rank t test.

5 min. After capturing the background signal for the initial 60 s, images were continuously taken while the fiber was washed with rigor buffer containing 4 mM ATP to flush mant-ATP for next 5 min. All images were taken by Hamamatsu 1394 ORCA-ERA camera at 20× objective power under DAPI filter (excitation 360 nm, emission 460 nm) equipped on a Leica DMi8 Widefield Fluorescence microscope every 5 s at room temperature 23 °C. Fluorescence intensity was measured in 2–3 different regions of fiber (50 μm × 50 μm) plus one background region. Individual fiber fluorescence intensity of each time point was subtracted from background intensity and normalized by the averaged baseline value prior to mant-ATP washout. To measure single myosin nucleotide (ATP) turnover, biphasic pulse-chase method was used, as previously described (53). All the results were fit to the double exponential decay to obtain $I = 1 - P_1(1 - e^{(-t)/T_1}) - P_2(1 - e^{(-t)/T_2})$, where I is the fluorescence intensity at any given time (t). P_1 is defined as the relative proportions of fluorescence in the first fast-phase exponent, and P_2 is defined as the relative proportions of fluorescence in the second slow-phase exponent. T_1 determines the lifetime of the first fast-phase exponent, and T_2 determines the lifetime of the second slow-phase exponent, which is the inverse of the rate of ATP turnover. The proportion of the SRX myosin is $2 \times P_2$, and the percentage of the DRX myosin is $1 - (2 \times P_2)$.

Loaded ATP turnover assays in permeabilized porcine single CMs

The ATP turnover rate of myosin in permeabilized single CMs under loaded conditions was conducted as described (32). Briefly, frozen porcine myocardium was cut into 10–15 mg pieces and permeabilized on ice in skinning solution (isolation buffer: 5.55 mM Na_2ATP, 7.11 M $MgCl_2$, 2 mM EGTA, 108.01 mM KCl, 8.91 KOH, 10 mM Imidazol, 10 mM DTT + 0.3% Triton X-100) with protease inhibitor cocktail (Sigma-Aldrich) and phosphatase inhibitors (PhosSTOP, Roche). The tissue was homogenized with low-speed pulverization, skinned for 20 min at 4 °C, and washed with isolation buffer to remove Triton. CMs were affixed to a force and length transducer using an ultraviolet-activated adhesive (Norland Optical Adhesives), and the sarcomere length was set to 2.1 μm. The CM was then washed in rigor buffer (6.41 mM $MgCl_2$, 10 mM EGTA, 100 mM N,N-Bis(2-hydroxyethyl)-2-aminoethanesulfonic acid (BES), 10 mM CrP, 50.25 mM K^+-propionate, protease inhibitor, 10 mM DTT) to remove ATP and subsequently incubated in relaxing buffer made with 25 μM 2′-/3′-*O*-(*N*′-methylanthraniloyl) adenosine-5′-*O*-triphosphate (mant-ATP, Enzo Life Sciences, Axxora LLC, Framingham, NY, USA). CMs were then moved to relaxing buffer and fluorescence intensity acquired (excitation 352–402 nm, emission 417–444 nm; Horiba/PTI 814 Photomultiplier Detection System) continuously at 100 Hz for 1,000 s at room temperature 23 °C. The fluorescence signal was filtered using a second-order Savitzky–Golay filter and normalized and fit to a double exponential function, as described above. Following the acquisition of the fluorescence decay curve, CMs were incubated in 1 μM OM and 7 μM piperine in relaxing solution for 10 min, and the assay repeated postexposure, with the chase performed in the presence of the drug. All analyses were performed using custom routines written in Matlab (Mathworks, 2020).

Funding

This project is supported by National Heart Lung and Blood Institute Grant (R01HL171657, W.M.), National Institute of Health predoctoral fellowship grant (F31 HL168850, V.P.J.); America Heart Associate predoctoral fellowship grant (23PRE1026275, V.P.J.), and career development award (23CDA1046498, T.S.). S.S. has received support from National Institutes of Health grants (R01 AR079435, R01 AR079477, R01 HL130356, R01 HL105826, R01 AR078001, and R01 HL143490), the American Heart Association, Institutional Undergraduate Student (25UFEL34380251), Transformation (945748) awards.

This research used resources from the Advanced Photon Source, a US Department of Energy (DOE) Office of Science User Facility operated for the DOE Office of Science by Argonne National Laboratory under Contract No. DE-AC02-06CH11357. This project is supported by grant P30 GM138395 from the National Institute of General Medical Sciences of the National Institutes of Health. The content is solely the authors' responsibility and does not necessarily reflect the official views of the National Institute of General Medical Sciences or the National Institutes of Health.

Author Contributions

W.M. designed the experiments; V.P.J., T.S., W.M., and H.G. performed the experiments; V.P.J., T.S., W.M., and C.G. analyzed the data; W.M., S.S., D.A.K., and T.C.I. wrote the manuscript. All authors approved the final version of the manuscript.

Preprints

This manuscript was posted on a preprint: https://doi.org/10.1101/2023.10.18.562891.

Data Availability

The datasets generated or analyzed during this study are all included in this article. The raw X-ray diffraction patterns in this study are deposited in the Zenodo repository (doi:10.5281/zenodo.10430839) and are available to the public.

References

1 Lehman W, Craig R, Vibert P. 1994. Ca^{2+} induced tropomyosin movement in *Limulus* thin filaments revealed by three-dimensional reconstruction. *Nature*. 368:65–67.
2 Risi CM, *et al.* 2021. The structure of the native cardiac thin filament at systolic Ca(2+) levels. *Proc Natl Acad Sci U S A*. 118: e2024288118.
3 Irving M. 2017. Regulation of contraction by the thick filaments in skeletal muscle. *Biophys J*. 113:2579–2594.
4 Hooijman P, Stewart MA, Cooke R. 2011. A new state of cardiac myosin with very slow ATP turnover: a potential cardioprotective mechanism in the heart. *Biophys J*. 100:1969–1976.
5 Cooke R. 2011. The role of the myosin ATPase activity in adaptive thermogenesis by skeletal muscle. *Biophys Rev*. 3:33–45.
6 Craig R, Padron R. 2022. Structural basis of the super- and hyper-relaxed states of myosin II. *J Gen Physiol*. 154:e202113012.
7 Anderson RL, *et al.* 2018. Deciphering the super relaxed state of human beta-cardiac myosin and the mode of action of mavacamten from myosin molecules to muscle fibers. *Proc Natl Acad Sci U S A*. 115:E8143–E8152.
8 Rohde JA, Roopnarine O, Thomas DD, Muretta JM. 2018. Mavacamten stabilizes an autoinhibited state of two-headed cardiac myosin. *Proc Natl Acad Sci U S A*. 115:E7486–E7494.
9 Spudich JA. 2019. Three perspectives on the molecular basis of hypercontractility caused by hypertrophic cardiomyopathy mutations. *Pflugers Arch*. 471:701–717.
10 Nag S, Trivedi DV. 2021. To lie or not to lie: super-relaxing with myosins. *Elife*. 10:e63703.
11 Kawana M, Spudich JA, Ruppel KM. 2022. Hypertrophic cardiomyopathy: mutations to mechanisms to therapies. *Front Physiol*. 13:975076.
12 Yuan CC, *et al.* 2022. Molecular basis of force-pCa relation in MYL2 cardiomyopathy mice: role of the super-relaxed state of myosin. *Proc Natl Acad Sci U S A*. 119:e2110328119.
13 Ho CY, *et al.* 2020. Evaluation of mavacamten in symptomatic patients with nonobstructive hypertrophic cardiomyopathy. *J Am Coll Cardiol*. 75:2649–2660.
14 Linari M, *et al.* 2015. Force generation by skeletal muscle is controlled by mechanosensing in myosin filaments. *Nature*. 528: 276–279.
15 Ma W, Irving TC. 2022. Small angle X-ray diffraction as a tool for structural characterization of muscle disease. *Int J Mol Sci*. 23:3052.
16 Huxley HE. 1973. Structural changes in actin- and myosin-containing filaments during contraction. *Cold Spring Harbor Symp Quant Biol*. 37:361–376.
17 Reconditi M, *et al.* 2005. Structure-function relation of the myosin motor in striated muscle. *Ann N Y Acad Sci*. 1047:232–247.
18 Huxley HE, Brown W. 1967. The low-angle X-ray diagram of vertebrate striated muscle and its behaviour during contraction and rigor. *J Mol Biol*. 30:383–434.
19 Huxley HE. 1971. Structural changes during muscle contraction. *Biochem J*. 125:85P.
20 Xu S, Offer G, Gu J, White HD, Yu LC. 2003. Temperature and ligand dependence of conformation and helical order in myosin filaments. *Biochemistry*. 42:390–401.
21 Caremani M, *et al.* 2019. Low temperature traps myosin motors of mammalian muscle in a refractory state that prevents activation. *J Gen Physiol*. 151:1272–1286.
22 Xu S, *et al.* 1997. X-ray diffraction studies of cross-bridges weakly bound to actin in relaxed skinned fibers of rabbit psoas muscle. *Biophys J*. 73:2292–2303.
23 Ma W, Duno-Miranda S, Irving T, Craig R, Padron R. 2021. Relaxed tarantula skeletal muscle has two ATP energy-saving mechanisms. *J Gen Physiol*. 153:e202012780.
24 Wilson C, Naber N, Pate E, Cooke R. 2014. The myosin inhibitor blebbistatin stabilizes the super-relaxed state in skeletal muscle. *Biophys J*. 107:1637–1646.
25 Morgan BP, *et al.* 2010. Discovery of omecamtiv mecarbil the first, selective, small molecule activator of cardiac myosin. *ACS Med Chem Lett*. 1:472–477.
26 Malik FI, *et al.* 2011. Cardiac myosin activation: a potential therapeutic approach for systolic heart failure. *Science*. 331:1439–1443.
27 Kampourakis T, Zhang X, Sun YB, Irving M. 2018. Omecamtiv mercabil and blebbistatin modulate cardiac contractility by perturbing the regulatory state of the myosin filament. *J Physiol*. 596:31–46.
28 Liu Y, White HD, Belknap B, Winkelmann DA, Forgacs E. 2015. Omecamtiv mecarbil modulates the kinetic and motile properties of porcine beta-cardiac myosin. *Biochemistry*. 54:1963–1975.
29 Woody MS, *et al.* 2018. Positive cardiac inotrope omecamtiv mecarbil activates muscle despite suppressing the myosin working stroke. *Nat Commun*. 9:3838.
30 Stewart MA, Franks-Skiba K, Chen S, Cooke R. 2010. Myosin ATP turnover rate is a mechanism involved in thermogenesis in resting skeletal muscle fibers. *Proc Natl Acad Sci U S A*. 107:430–435.
31 Wilson C, Naber N, Cooke R. 2021. The role of the super-relaxed state of myosin in human metabolism. *Metabol Open*. 9:100068.
32 Jani V, Qian W, Yuan S, Irving T, Ma W. 2022. EMD-57033 augments the contractility in porcine myocardium by promoting the activation of myosin in thick filaments. *Int J Mol Sci*. 23:14517.
33 Ranu N, *et al.* 2022. NEB mutations disrupt the super-relaxed state of myosin and remodel the muscle metabolic proteome in nemaline myopathy. *Acta Neuropathol Commun*. 10:185.
34 Ma W, *et al.* 2021. The super-relaxed state and length dependent activation in porcine myocardium. *Circ Res*. 129:617–630.

35 Jani V, *et al.* 2023. Right ventricular sarcomere contractile depression and the role of thick filament activation in human heart failure with pulmonary hypertension. *Circulation*. 147:1919–1932.
36 Ma W, *et al.* 2023. Structural OFF/ON transitions of myosin in relaxed porcine myocardium predict calcium activated force. *Proc Natl Acad Sci U S A*. 120:e2207615120.
37 Walklate J, Kao K, Regnier M, Geeves MA. 2022. Exploring the super-relaxed state of myosin in myofibrils from fast-twitch, slow-twitch and cardiac muscle. *J Biol Chem*. 298:101640.
38 Chu S, Muretta JM, Thomas DD. 2021. Direct detection of the myosin super-relaxed state and interacting-heads motif in solution. *J Biol Chem*. 297:101157.
39 Padron R, *et al.* 2020. The myosin interacting-heads motif present in live tarantula muscle explains tetanic and posttetanic phosphorylation mechanisms. *Proc Natl Acad Sci U S A*. 117:11865–11874.
40 Dutta D, Nguyen V, Campbell KS, Padrón R, Craig R. 2023. Cryo-EM structure of the human cardiac myosin filament. bioRxiv 536274. https://doi.org/10.1101/2023.04.11.536274, preprint: not peer reviewed.
41 Ma W, Nag S, Gong H, Qi L, Irving T. 2022. Cardiac myosin filaments are directly regulated by calcium. *J Gen Physiol*. 154:e202213213.
42 Mohran S, *et al.* 2023. The biochemically defined super relaxed state of myosin—a paradox. *J Biol Chem*. 300:105565.
43 Dutta D, Nguyen V, Campbell KS, Padron R, Craig R. 2023. Cryo-EM structure of the human cardiac myosin filament. *Nature*. 623:853–862.
44 Tamborrini D, *et al.* 2023. Structure of the native myosin filament in the relaxed cardiac sarcomere. *Nature*. 623:863–871.
45 Ma W, *et al.* 2022. Myofibril orientation as a metric for characterizing heart disease. *Biophys J*. 121:565–574.
46 Ma W, *et al.* 2023. The structural and functional integrities of porcine myocardium are mostly preserved by cryopreservation. *J Gen Physiol*. 155:e202313345.
47 Fischetti R, *et al.* 2004. The BioCAT undulator beamline 18ID: a facility for biological non-crystalline diffraction and X-ray absorption spectroscopy at the advanced photon source. *J. Synchrotron Radiat*. 11:399–405.
48 Jiratrakanvong J, *et al.* 2018. MuscleX: software suite for diffraction X-ray imaging V1.21.0. https://doi.org/10.5281/zenodo.1195050
49 Ma W, Gong H, Irving T. 2018. Myosin head configurations in resting and contracting murine skeletal muscle. *Int J Mol Sci*. 19:2643.
50 Ma W, *et al.* 2018. Thick-filament extensibility in intact skeletal muscle. *Biophys J*. 115:1580–1588.
51 McNamara JW, *et al.* 2017. MYBPC3 mutations are associated with a reduced super-relaxed state in patients with hypertrophic cardiomyopathy. *PLoS One*. 12:e0180064.
52 McNamara JW, *et al.* 2016. Ablation of cardiac myosin binding protein-C disrupts the super-relaxed state of myosin in murine cardiomyocytes. *J Mol Cell Cardiol*. 94:65–71.
53 Cooke R, Pate E. 1985. The effects of ADP and phosphate on the contraction of muscle fibers. *Biophys J*. 48:789–798.